UCRL- 92202
PREPRINT

A MODEL TO CALCULATE ATOMIC SPECTRA IN HOT PLASMAS

A. Goldberg, B. F. Rozsnyai, and P. Thompson
University of California, Lawrence Livermore National Laboratory
Livermore, California 94550

This paper was prepared for submittal to
Physical Review A

February 20, 1985

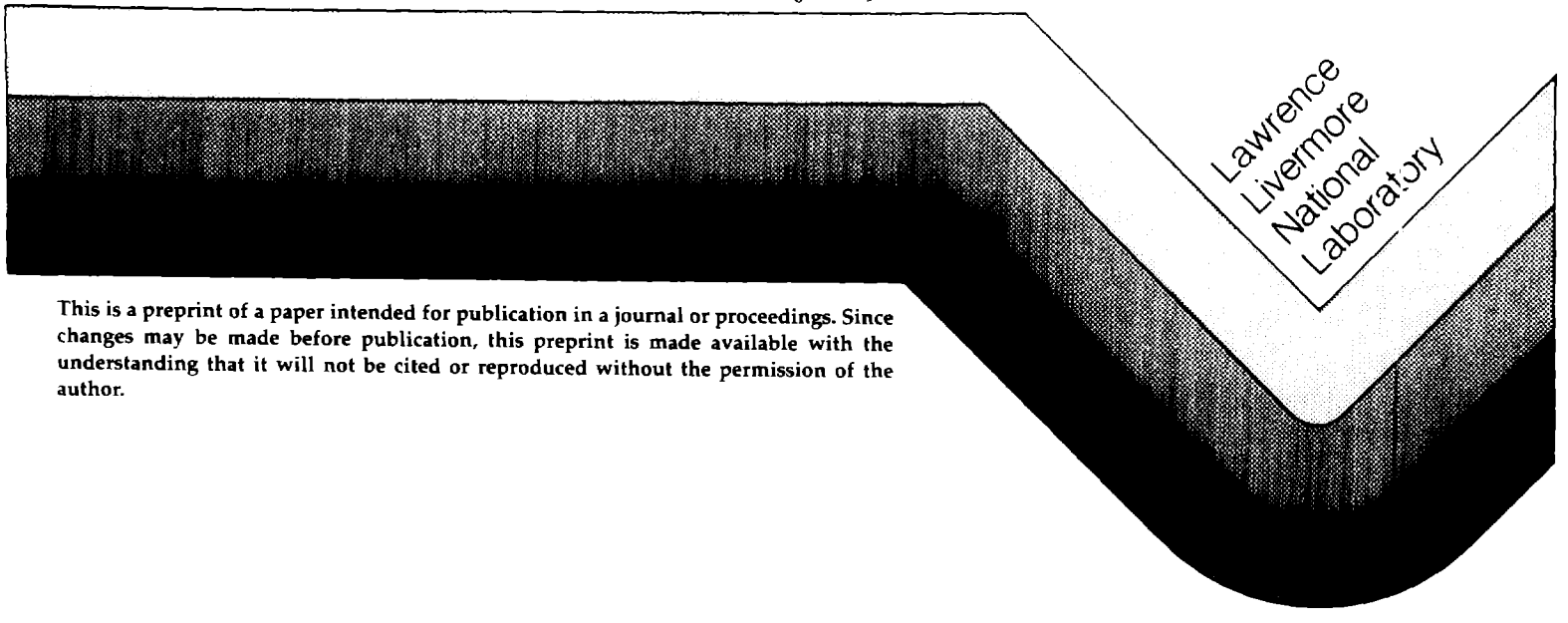

A Model to Calculate Atomic Spectra in Hot Plasmas*

A. Goldberg, B. F. Rozsnyai, and P. Thompson
University of California, Lawrence Livermore National Laboratory
Livermore, California 94550

Abstract

An algorithm is presented for the detailed computation of transition arrays in hot, partially ionized plasmas. The method is illustrated for bromine plasma at temperatures and densities when partially filled L and M shells occur.

*Work performed under the auspices of the U.S. Department of Energy by Lawrence Livermore National Laboratory under contract #W-7405-Eng-48.

I. Introduction

The proper accounting of the large number of spectral lines in hot, partially ionized matter is important for opacities and also for plasma diagnostics. E. Teller[1] first recognized the importance of line opacities in hot matter, subsequently rediscovered by many other researchers. The strong effect of dispersed line clusters on the Rosseland mean opacity of partially ionized gold was demonstrated by Nardi and Zinamon.[2] A brief quantitative illustration of the relative importance of line and continuus opacities for iron plasma was also given by Rozsnyai.[3] Theoretical estimates for the degree of dispersion of line clusters due to the different angular momentum states of the many electron system were give by Moszkowski,[4] and more recently in a series of reports by Bauche, et al.[5-7].

Although the estimate of the degree of dispersion of lines due to the different angular momentum states is important, a detailed accounting of lines is necessary for accurate opacity calculations and also to predict expected spectral patterns. Whether or not the line clusters actually merge into continuous profiles depends on the physical line-broadening characteristics of the plasma, so that line broadening is an integral part of the spectroscopic model. The main objective of this paper is to describe a computational procedure for the accounting of large number of spectral lines in medium Z plasmas at temperatures such that partial ionization occurs. Since the computation problem is enormous, approximations are a practical necessity. Presently we use first order perturbation theory for the computation of spectroscopic terms in the LS coupling scheme. We present some calculations for bromine plasma at temperatures and densities corresponding to partially

filled L and M shells. Also, for the present, we limit our model to conditions of local thermodynamic equilibrium (LTE). In Section II we present the theoretical basis of our model and in Section III we present some computational results.

II. Theory

The theoretical basis of our model is the utilization of the "average atom" (AA) wave functions to compute the expectation values of our model Hamiltonian. These expectation values are computed for eigenstates of the L^2 and S^2 operators of the many electron system. The AA model, which is the starting point of our computational procedure, is described by Rozsnyai[8], and in references given there; here we merely recall the rudiments of that model.

The AA model assumes that the electronic levels in the plasma are populated according to the Fermi statistics

$$q_{nl} = g_{nl}\{\exp[-(e_{nl}-\mu)/kT]+1\}^{-1} \tag{1}$$

where q_{nl} and g_{nl} are the population and statistical weight of a single particle level with energy e_{nl} and with quantum numbers n and l, μ is the Fermi level and kT is the temperature in energy units. The electronic potential is assumed to be spherically symmetric and the radial part of the single particle wave functions satisfy Schrodinger's equation (in atomic units)

$$R''_{nl} + 2R'_{nl}/r + \{2[e_{nl}-V(r)]-l(l+1)/r^2\}R_{nl} = 0. \tag{2}$$

In Eq. (2) the electronic potential is given by

$$V(r) = -Z/r + \int d^3r' \frac{\rho(r')}{|r-r'|} + V_{xc}[\rho(r)] \qquad (3)$$

where Z stands for the charge of the nucleus and the electron density is given by

$$\rho(r) = \sum_{n,\ell} q_{n\ell} |R_{n\ell}(r)|^2 \quad . \qquad (4)$$

The last term in Eq. (3) stands for the exchange-correlation part, approximated by a local potential which is a unique functional of the electron density. In our model for V_{xc} we adopt the formula of Hedin and Lundqvist.[9]

It should be noted that in Eq. (4) the summation goes over all states, including the continuum. Because of that, our model includes the screening effect by the continuum electrons also. The actual computation technique to account for the free electrons is described in Ref.8.

For a given temperature the Fermi level μ is determined by the condition of charge neutrality

$$\int_0^{r_o} \rho(r)\, r^2 dr = Z \quad , \qquad (5)$$

where r_0 stands for the ion sphere radius determined by the matter density.

Equations 1-5 give a complete self-consistent set of equations for the AA model. Its shortcoming is that at finite temperature it predicts non-integer occupation numbers for the electronic levels, making the physical state of the AA fictitious. The usefulness of the AA model extends to the degree of its usefulness as a statistical average.

We proceed by separating the electronic levels of the AA into core and valence states. Core states are those for which $q_{nl} \sim g_{nl}$ which is the case for energy levels well below the Fermi level. Valence states are those with fractional or near zero occupational numbers. We create concrete physical electronic states involving the valence states in the following manner:

First, we truncate the AA occupational numbers to their nearest integer values, creating the "most probable atom". In contrast to the AA, the "most probable" atom is not fictitious but a physically permissible specimen. Next, we create different electronic configurations from the "most probable" atom by promoting and demoting electrons in the valence levels. We also create different charge states by increasing or decreasing the number of valance electrons and repeat the same procedure. For each configuration we create all the possible L and S states by diagonalizing the L^2 and S^2 operators.

Since we are faced with an enormous number of possible states we restrict ourselves to those with appreciable probability. The procedure described above is carried out for the "parent" and "daughter" configurations. Parent and daughter configurations are distinguished by promoting an electron from a nl state to an upper n'l' state due to photoabsorption. A somewhat similar calculational method has been given by Argo and Huebner,[10] where the energies of th LS states were not resolved, and also the configurational energies utilized Slater integrals Z scaled for isolated ions. More recently Goldberg and Rozsnyai[11] gave results from a simplified version of the model described in this paper where only the lower parent configurations were energy resolved.

Our model Hamiltonian used for the computation of term energies and for the probabilities of the parent states is given by

$$H = H_0 + \frac{1}{2} \sum_{i,j} \frac{1}{r_{ij}} \tag{6}$$

with i and j covering the valence electrons only, and

$$H_0 = \sum_i \left[-\frac{\hbar^2}{2m} \nabla_i^2 - \frac{Z}{r_i} + V_c(r_i) \right] . \tag{7}$$

The term V_c in Eq. (7) stands for the "core" potential due to the charge distribution of the core electrons, and is given by

$$V_c(r) = \int d^3r' \frac{\rho_c(r)}{|r-r'|} + V_{xc}[\rho_c(r)] \tag{8}$$

with

$$\rho_c(r) = \sum_c g_{nl} |R_{nl}(r)|^2$$

and the summation goes over to the core states. We compute the expectation values of the Hamiltonian (6) for all parent and daughter states which are eigenstates of the L^2 and S^2 operators. Since the Hamiltonian (6) involves the valence electrons only, the self energy of the core is unaccounted . For the computation of transition energies between parent and daughter states due to photoabsorption the core self-energy cancels out to the extent that core polarization is negligible.

We thus construct linear combinations of Slater determinental wave functions, the determinents comprised of the single particle orbitals for the valence electrons. These linear combinations are chosen to simultaneously diagonalize $L^2 = (\sum \bar{\ell}_i)^2$, $S^2 = (\sum \bar{s}_i)^2$ and H [Eq. (6)], with the subspace of one configuration, where of course the sums are taken over the valence electrons only. This diagonalization is performed directly and does not utilize tables of c.f.p.s, etc. This program is quite fast and presently can treat configurations containing over 400 separate term values.

If we label the expectation value of the Hamiltonian (6) for a L S state in a certain configuration α by $E(L,S,\alpha)$, then the probability of that state under LTE condition is given by

$$P(L,S,\alpha) = KG(L,S) \exp\left\{ - \frac{E(L,S,\alpha) - \mu N_v}{kT} \right\} \qquad (3)$$

where N_v is the number of valence electrons in the configuration α. In Eq. (9), G(L,S) is the statistical weight (2L+1)(2S+1) and the constant K is determined by the normalization condition

$$\sum_{LS\alpha} P(L,S,\alpha) = 1 \quad .$$

In Eq. (9) α stands for a particular configuration of the N_v valence electrons distributed over the valence states.

Our aim is to account for all the lines of a cluster associated with a single electron transition of the type nl→n'l', where the members of a cluster differ by belonging to different parent configurations and/or LS states. The transition energy of a particular line is

$$E(L',S,\alpha')-E(L,S,\alpha) \tag{10}$$

with the selection rule $\Delta L = 0,+1$, α and α' differ in the occupation number of the one electron states nl, n'l' by one. To obtain the desired spectra we computed all the relevant term energies and oscillator strengths for all the transitions of the type in Eq. (10), together with the probabilities of the parent states as given by Eq. (9).

Since our model calculations are done in the LS coupling scheme, it may not be adequate for medium or large Z plasmas when the spin-orbit interaction becomes significant. For this reason we add the spin orbit interaction to the transition energies given by Eq. (10) in the single-particle approximation by the operator

$$H_{S.O} = \frac{\hbar^2}{4m^2c^2} \sum_i \frac{1}{r_i} \frac{dV(r_i)}{dr_i} (\bar{\ell}_i \cdot s_i) \qquad (11)$$

where the summation goes over all the valence electron coordinates and the electron potential V(r) in Eq. (11) is the AA potential. This corresponds to correcting the transition energies given by Eq. (10) with the single-electron spin-orbit energy shifts of the AA model. In this approximation of the spin-orbit interaction each spectral line breaks up into three (or two, if one of the single electron sates is an s state), and, accordingly the oscillator strengths must be multiplied by the factors a,b,c[12] where

$$a:b:c = (\ell+2)(2\ell+1):1:(\ell+1)(2\ell+3) \qquad (12a)$$

for $\ell \rightarrow \ell+1$ transitions and

$$a:b:c: = \ell(2\ell-1):1:(\ell-1)(2\ell+1) \qquad (12b)$$

for $\ell \rightarrow \ell-1$ Transitions.

The oscillator strengths and term energies are calculated using the AA wave functions as the basis single particle set for our many-body representation. In this sense our model is a first order perturbation calculation using the self-consistent AA model as a start.

In order to obtain a meaningful spectroscopic result the bound-bound oscillator strengths have to be supplied with reasonable line shape profiles to compute frequency dependent absorption cross sections. In a real plasma

the bound-bound cross sections are superimposed on the bound-free and free-free, which are also to be taken into account. The computation of spectrum profiles, bound-free and free-free processes is described by Rozsnyai[13-16] and the reader is referred to the quoted references. In the next Section we illustrate our model by presenting some calculations for bromine plasma.

III. Numerical Calculations

We illustrate the case of partially filled L-shells for the bromine plasma at density 5.10^{-2}g/cc and at temperatures kT = 280 and 350 eV, respectively. In the first case the AA model predicts an almost filled L-shell and in the second case a half-filled L-shell. In our detailed spectroscopic accounting in the first case we calculated 15 parent LS states from nitrogen -like to neon- like ions with neon-like and fluorine- like ions having the largest probabilities, as illustrated in Table I. In the second case the number of parent LS states were 41 going from berrylium-like to fluorine-like ions with the probability distribution peeking at the nitrogen-like states. We accounted for all the n = 2→3 and 2→4 transition arrays which before the spin-orbit splitting gave us 404 lines for the first case and 840 for the second. After taking into account the spin-orbit interaction in the single-particle approximation as described above, having supplied the lines with reasonable line-shape profiles and having computed the bound-free and free-free absorption cross-sections, as described in Refs.11-14, we computed the total photoabsorption cross section for the plasma, with results shown in Figs. 1 and 2. We also predict the emission spectrum from an optically thin plasma by taking the simplest solution of the radiative transfer equation

$$I(\nu) = B(\nu) \{ 1 - \exp [\sigma(\nu)\rho L]\} \qquad (13)$$

where $I(\nu)$ is the intensity of the emerging radiation, $B(\nu)$ is the Planck function, $\sigma(\nu)$ the frequency dependent photoabsorption cross section, as indicated in Figs. 1-2, ρ is the matter density and L is the thickness of the sample through which the radiation must pass before emerging. The results of these calculations are shown in Figs. 3 and 4 on the linear scale to compare our data with experimental measurements.

At present no experiments are known to the authors for LTE plasmas. In the case of laser or electron-beam produced plasmas only the free electrons, which are usually Maxwellian, have the property of a temperature, and the bound electrons within the ions are distributed according to the collision-radiative rate equations. Therefore, it is rather difficult to correlate our LTE model with the available experimental data. Nevertheless we attempt to do that by chosing the temperature-density conditions so that the LTE distribution of the different ionic species is close to those of the non-LTE experimental conditions. In Fig. 5 we show the experimental measurements of Bailey, et al.[17] for laser produced bromine plasma. The free-electron density and temperature were estimated as 10^{22} cm^{-3} and 500 eV, respectively, and the plasma is mainly neon-like and optically thin. To mimic these conditions with our LTE model we chose the same electron density, corresponding to 5.10^{-2} g/cc matter density, and to make the plasma mainly neon and fluorine-like, we took the temperature as 280 eV. For the sample thickness L we chose 3.5 10^{-4}cm which corresponds to the experimental conditions. A comparison of Figs.3 and 5 shows that the calculated strong lines have about the same wavelengths as those in the experiment, while the

strength ratios seem to be different. This difference is not surprising in view of the difference between LTE and non-LTE conditions. Presently we have no experimental data to compare our calculations for 350 eV corresponding to Figs. 2 and 4. The results at 350 eV temperature are given only to illustrate the effect of the increasing number of spectral lines.

We show some of the spectroscopic details in Table I and in Figs. 6 and 7. Table I shows the 15 parent states with their probabilities for the 280 eV calculation of the bromine plasma. From these parent states we included all the n = 2-3 and 2-4 arrays. For the 2p-3d array we show the oscillator strengths multiplied with the probability of the respective parent states in Fig. 6. In Fig. 7 we show the same as in Fig. 6 at 350 eV temperature.

In Tables II and III we compare briefly the data predicted by the AA model with those of our detailed spectroscopic accounting. In column 2 the transition energy E(aa) is simply the difference of the single particle energy levels as predicted by the self-consistent AA model. In column 3 E(a) is the average transition energy of a nl-n'l' array given by

$$\Delta E_{n\ell\to n'\ell'}(a) = \sum_{\alpha,\alpha'} P(\alpha) f(\alpha\to\alpha') \Delta E(\alpha\to\alpha;) f_{n\ell\to n'\ell'}(a) \qquad (14)$$

where the summation goes over all the parent LS states labelled by α and over all the daughter LS states labelled by α' which differ from the parent states by changing one electron from an nl to an n'l' single particle state. In Eq. (14) $P(\alpha)$ is the probability of the parent state, $f(\alpha\to\alpha')$ is the

oscillator strength of the transition and ΔE is the energy difference. The last term in Eq. (14) is the average oscillator strength for an nl-n'l' transition array given by

$$f_{n\ell\to n'\ell'}(a) = \sum_{\alpha\alpha'} P(\alpha) f(\alpha\to\alpha') \qquad (15)$$

and are shown in column 7 in Tables II and III. The oscillator strength for an $n\ell$-$n'\ell'$ transition predicted by the AA model is given by

$$f_{n\ell\to n'\ell'}(aa) = \frac{2}{3}\Delta E_{n\ell\to n'\ell'}(aa)\, q_{nl}\, \frac{\ell_>}{2\ell+1}\, |D(n\ell\to n'\ell')|^2 \qquad (16)$$

where q_{nl} is the occupation number of the shell nl as given by Eq. (1) and D stands for the dipole radial integral. The AA oscillator strengths are shown in columns 7 in Tables II and III. It should be noted that we use the same dipole radial integrals needed for the AA and detailed LS oscillator strengtns by using the AA radial wave functions, so the difference between the f(aa) and f(a) quantities is due to the statistics only. In columns 5 and 6 we also give the second and third momemnts of the distribution of lines within an array by using the formula for the $\underline{k}$ th moments

$$\Delta^k(n\ell\to n'\ell') = \sum_{\alpha,\alpha'} P(\alpha)[\Delta E(\alpha\to\alpha') - \Delta E_{n\ell\to n'\ell'}(a)]^k \times f^{-1}_{n\ell\to n'\ell'}(a) \,. \qquad (17)$$

The fact that the third moments are not small indicates that the line distributions are not symmetric around the average as in a simple Gaussian model.

At kT = 60 eV, the dominant parent configurations all have partially filled M-shells, and at density = 5.10^{-2}g/cc, 34 parent configurations have significant probability. The two most probable initial configurations are $[Ne](3s^2)(3p^6)(3d^5)$ and $[Ne](3s^2)(3p^5)(3d^4)$. Figures 8 and 9 exhibit the transition arrays generated by promoting an electron in these configurations from the 3d to the 4f level. These arrays contain respectively 438 and 5523 line transitions and they are by no means the largest that need to be treated. Inclusion of all parent configurations and all parent LS states, as was done for the L-shell spectra, simply exceeds our computational ability. One might consider modeling these transition arrays using the first three moments give by Refs. 5-7. Figures 8 and 9 indicate, however, that these arrays are characterized by a broad almost continuous background of many lines, but upon which is superposed a discrete structure of relatively few intense lines. Since there is no a priori procedure to determine the positions and strengths of these intense lines, there remains no recourse to the prediction of these arrays other than brute force computation.

In summary, the algorithm described in this paper is easily applicable to LTE spectra for partially filled L-shells (and of course, K-shells), while for M-shells and above, the procedure becomes lengthy and laborious. We are aware that LTE conditions are difficult to achieve in laboratory conditions; nevertheless, it is hoped that spectroscopic data from LTE plasmas will become available for comparison with theoretical predictions.

Acknowledgement

The authors are grateful to Ms. R. Walling for the several useful discussions, and we thank her and her coauthors of Ref. 17 for their permission to reproduce Fig. 5.

AG:SN:mpd:0014t

Table I. List of parent states and probabilities in bromine plasma at kT = 280 eV and at $\rho = 5.10^{-2}$g/cc.

State	Probability
[Ne]	3.507(-1)
[He]$(2s^1)(2p^6)$2S	6.932(-2)
[He]$(2s^2)(2p^5)$2P	3.995(-1)
[He]$(2s^1)(2p^5)$1P	1.089(-2)
[He]$(2s^1)(2p^5)$3P	3.943(-2)
[He]$(2s^2)(2p^4)$1S	6.528(-3)
[He]$(2s^2)(2p^4)$3P	6.897(-2)
[He]$(2s^2)(2p^4)$1D	3.594(-2)
[He]$(2s^1)(2p^4)$2P	1.518(-3)
[He]$(2s^1)(2p^4)$2S	5.205(-4)
[He]$(2s^1)(2p^4)$4P	4.029(-3)
[He]$(2s^1)(2p^4)$2D	2.865(-3)
[He]$(2s^2)(2p^3)$2P	2.732(-3)
[He]$(2s^2)(2p^3)$2D	4.855(-3)
[He]$(2s^2)(2p^3)$4S	2.139(-3)

Table II. Energies, variances in eV and oscillator strengths for transition arrays in bromine plasma at kT = 280 eV and at $\rho = 5.10^{-2}$g/cc.

Array	ΔE(aa)	ΔE(a)	$[\Delta^2]^{1/2}$	$[\Delta^3]^{1/3}$	f(aa)	f(a)
2s-3p	1.841(3)	1.873(3)	4.381(1)	4.132(1)	5.744(-1)	6.287(-1)
2s-4p	2.362(3)	2.409(3)	6.576(1)	5.808(1)	1.549(-1)	1.665(-1)
2p-3s	1.630(3)	1.646(3)	5.434(1)	4.667(1)	8.405(-2)	8.738(-2)
2p-3d	1.748(3)	1.780(3)	4.622(1)	4.051(1)	2.964	3.233
2p-4s	2.182(3)	2.212(3)	7.442(1)	6.337(1)	1.909(-2)	1.962(-2)
2p-4d	2.228(3)	2.265(3)	7.353(1)	6.326(1)	6.416(-1)	6.862(-1)

Table III. Energies, variances in eV and oscillator strengths for transition arrays in bromine plasma at kT = 350 eV and at $\rho = 5.10^{-2}$ g/cc.

Array	ΔE(aa)	ΔE(a)	$[\Delta^2]^{1/2}$	$[\Delta^3]^{1/3}$	f(aa)	f(a)
2s-3p	1.949(3)	1.964(3)	6.024(1)	3.022(1)	4.757(-1)	5.163(-1)
2s-4p	2.536(3)	2.565(3)	9.065(1)	4.131(1)	1.253(-1)	1.345(-1)
2p-3s	1.768(3)	1.774(3)	8.162(1)	4.044(1)	5.641(-2)	5.172(-2)
2p-3d	1.867(3)	1.881(3)	6.308(1)	2.543(1)	2.213	2.364
2p-4s	2.381(3)	2.401(3)	1.119(2)	5.331(1)	1.338(-2)	1.224(-2)
2p-4d	2.420(3)	2.443(3)	1.020(2)	4.225(1)	4.580(-1)	4.835(-1)

REFERENCES

1. See Harris Mayer, "Methods of Opacity Calculations" page 2, Los Alamos Report 647 (1947).

2. E. Nardi and Z. Zinamon, Phys Rev. A 20, 1197, (1979).

3. B. F. Rozsnyai, JQSRT 27, 211 (1981).

4. S. A. Moszkowski, Prog. Theor. Phys. 28, 1, (1962).

5. C. Bauche-Arnoult, J. Bauche and M. Klapisch, Phys. Rev. A 20, 2424 (1979).

6. C. Bauche-Arnoult, J. Bauche and M. Klapisch, Phys. Rev. A 25, 2641 (1982).

7. J. Bauche, C. Bauche-Arnoult, E. Luc-Koenig, J. F. Wyart and M. Klapisch, Phys. Rev. A 28, 829, (1983).

8. B. F. Rozsnyai, Phys. Rev. 145, 1137 (1972).

9. L. Hedin and B. I. Lundqvist, J. Phys. C 4, 2064 (1971).

10. M. F. Argo and W. F. Huebner, JQSRT 16, 1091 (1976).

11. A. Goldberg and B. F. Rozsnyai, Proceedings of the Second International Conference on Radiative Properties of Hot Dense Matter, Sarasota Florida Oct 31-Nov. 1 1982, in press.

12. See Bethe and Salpeter, Quantum Mechanics of One-and Two-Electron Systems p. 273, Springer (1957). Note that the ratios for oscillator strengts are not the same as those for the transition strengths.

13. B. F. Rozsnyai, JQSRT 17, 77 (1977).

14. B. F. Rozsnyai, JQSRT 19, 641 (1978).

15. B. F. Rozsnyai, JQSRT 13, 1285 (1973).

16. B. F. Rozsnyai, JQSRT 22, 337 (1979).

17. J. Bailey, R. E. Stewart, R. J. Fortner, J. Kilkenney, R. W. Lee, T. Phillips and R. Walling, to be published.

Figure Captions

FIG. 1 Computer output of photoabsorption cross section in units of cm ^{2}/g versus photon energy in eV of bromine at kT = 280 eV temperature and at $\rho = 5.10^{-2}$ g/cc density.

FIG. 2 Same as Fig. 1 at kT = 350 eV temperature.

FIG. 3 Estimated emission intensity versus wavelength of bromine plasma corresponding to the temperature-density conditions of Fig. 1 and sample thickness of $3.5\ 10^{-4}$ cm.

FIG. 4 Same as Fig. 3, but corresponding to the temperature-density condition of Fig. 2.

FIG. 5 Experimental measurement of emission from neon-like and fluorine-like bromine plasma as taken from Ref. 17.

FIG. 6 Computer output for the weighted oscillator strengths for the 2p-3d array of bromine plasma corresponding to the temperature-density condition of Fig. 1. The total number of 2p-3d lines is 86.

FIG. 7 Same as Fig. 6., but corresponding to the temperature density condition of Fig. 2. The total number of 2p-3d lines is 184.

FIG. 8 Array of oscillator strengths for the 3d-4f single electron transitions from the $[Ne](3s^2)(3p^5)(3d^4)$ parent configuration for bromine plasma at $\rho = 5.10^{-2}$ g/cc and at kT = 60 eV temperature.

FIG. 9 Same as Fig. 8 from the $[Ne](3s^2)(3p^6)(3d^5)$ parent configuration.

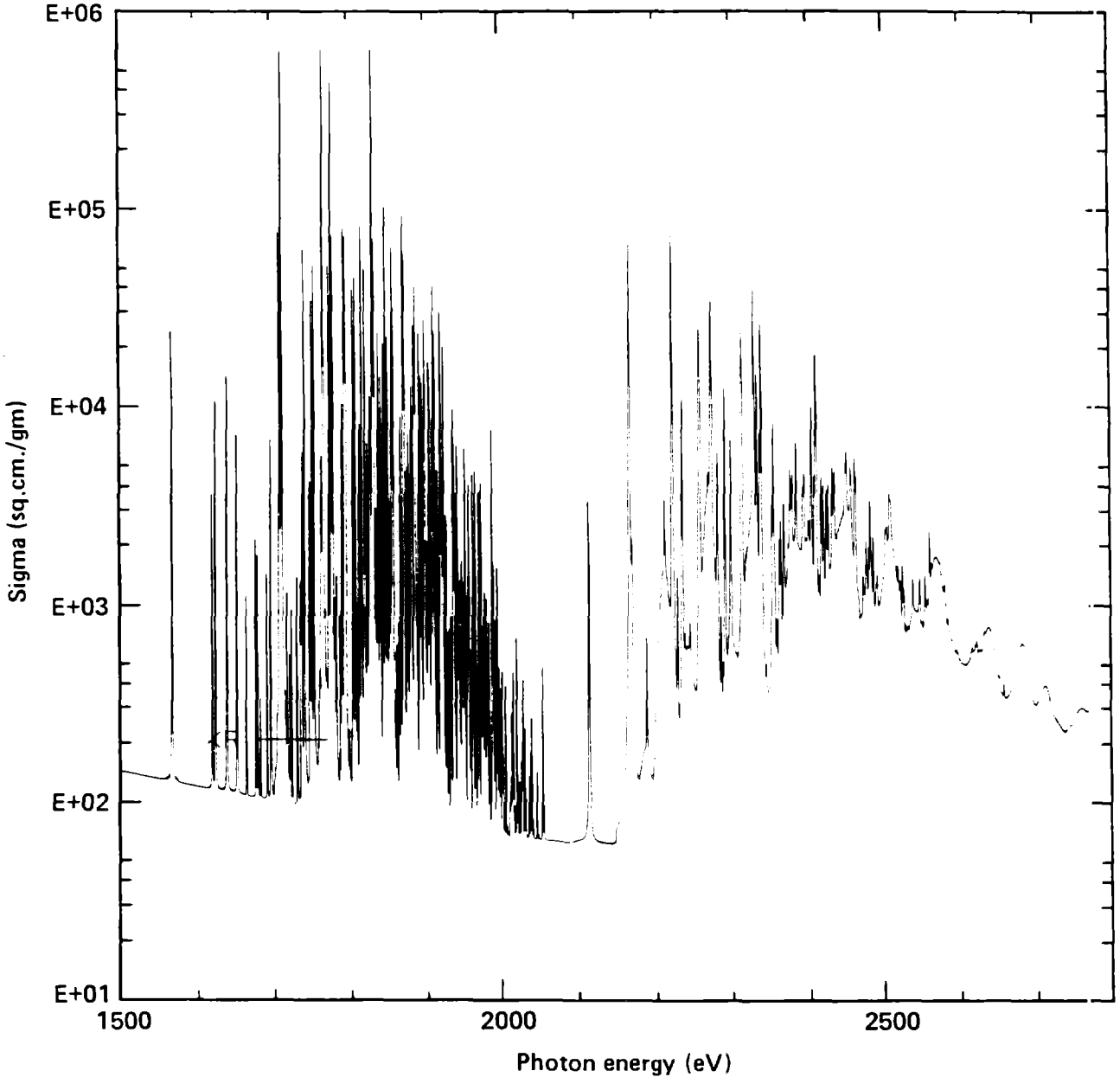
E+06
E+05
E+04
E+03
E+02
E+01
Sigma (sq.cm./gm)
1500
2000
2500
Photon energy (eV)

Fig. 1

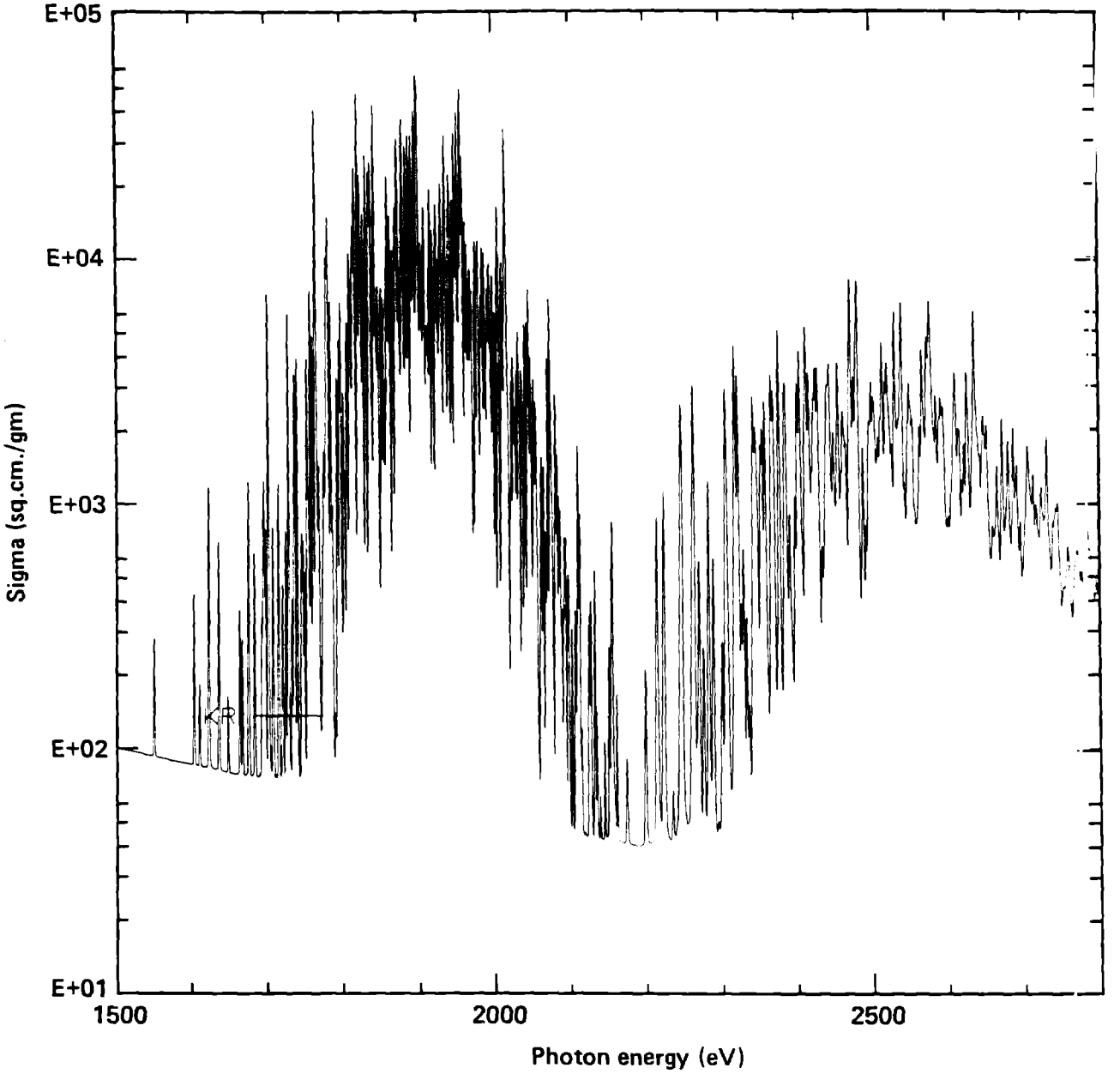
E+05
E+04
E+03
E+02
E+01
Sigma (sq.cm./gm)
1500
2000
2500
Photon energy (eV)
KR

Fig. 2

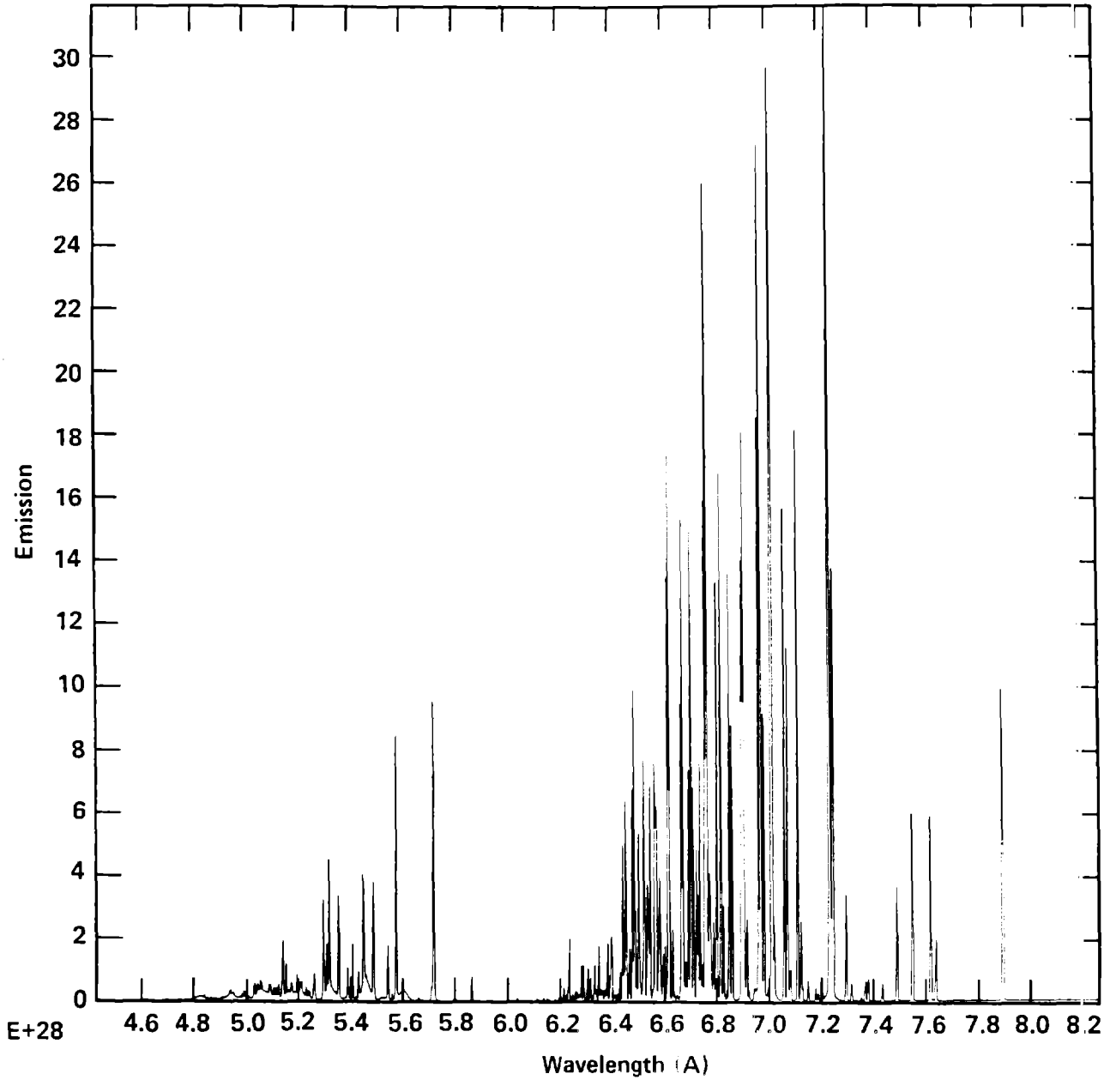
30
28
26
24
22
20
18
16
14
12
10
8
6
4
2
0
Emission
E+28
4.6 4.8 5.0 5.2 5.4 5.6 5.8 6.0 6.2 6.4 6.6 6.8 7.0 7.2 7.4 7.6 7.8 8.0 8.2
Wavelength (A)

Fig. 3

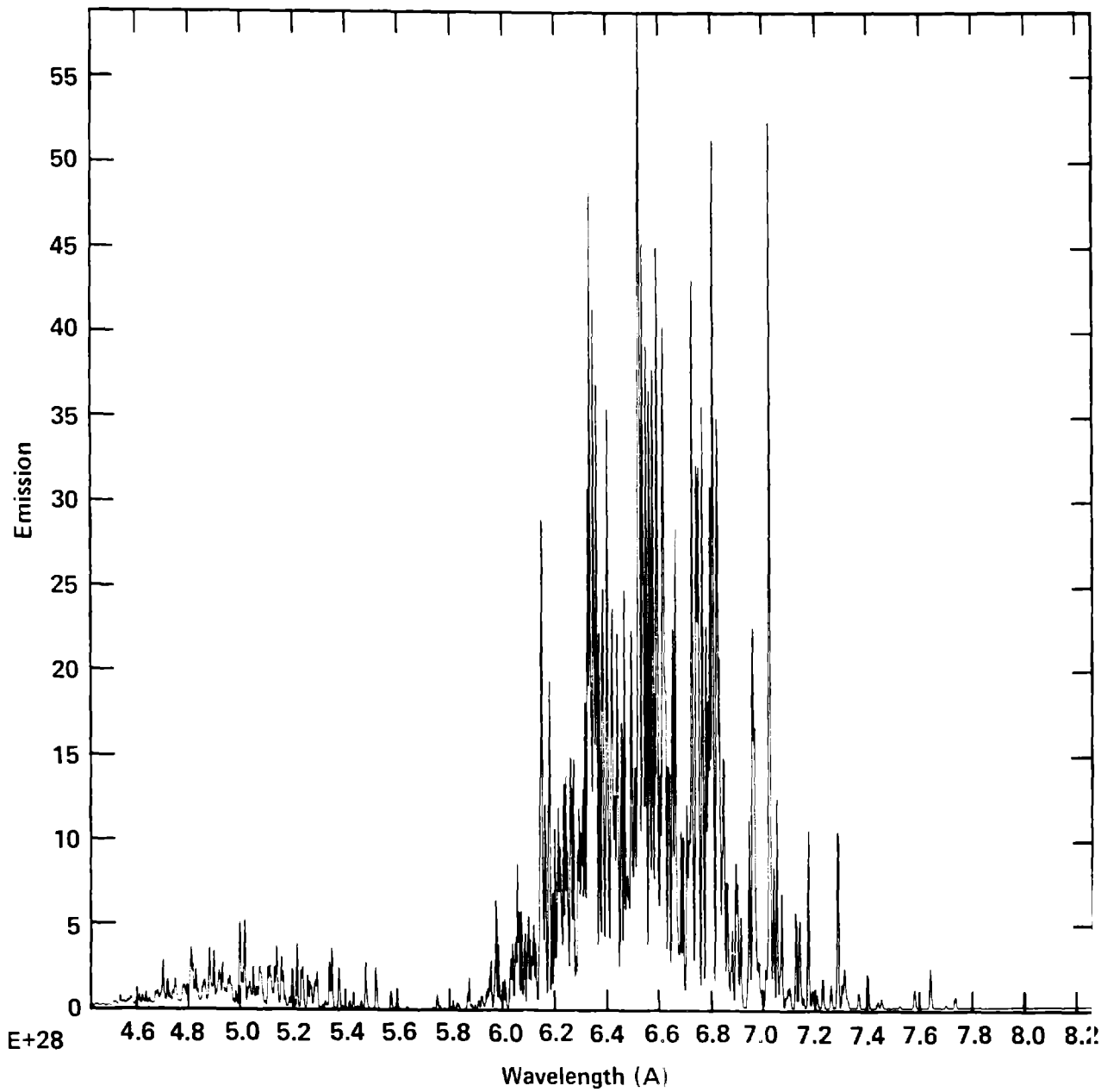
55
50
45
40
35
30
25
20
15
10
5
0
Emission
E+28
4.6 4.8 5.0 5.2 5.4 5.6 5.8 6.0 6.2 6.4 6.6 6.8 7.0 7.2 7.4 7.6 7.8 8.0
Wavelength (A)

Fig. 4

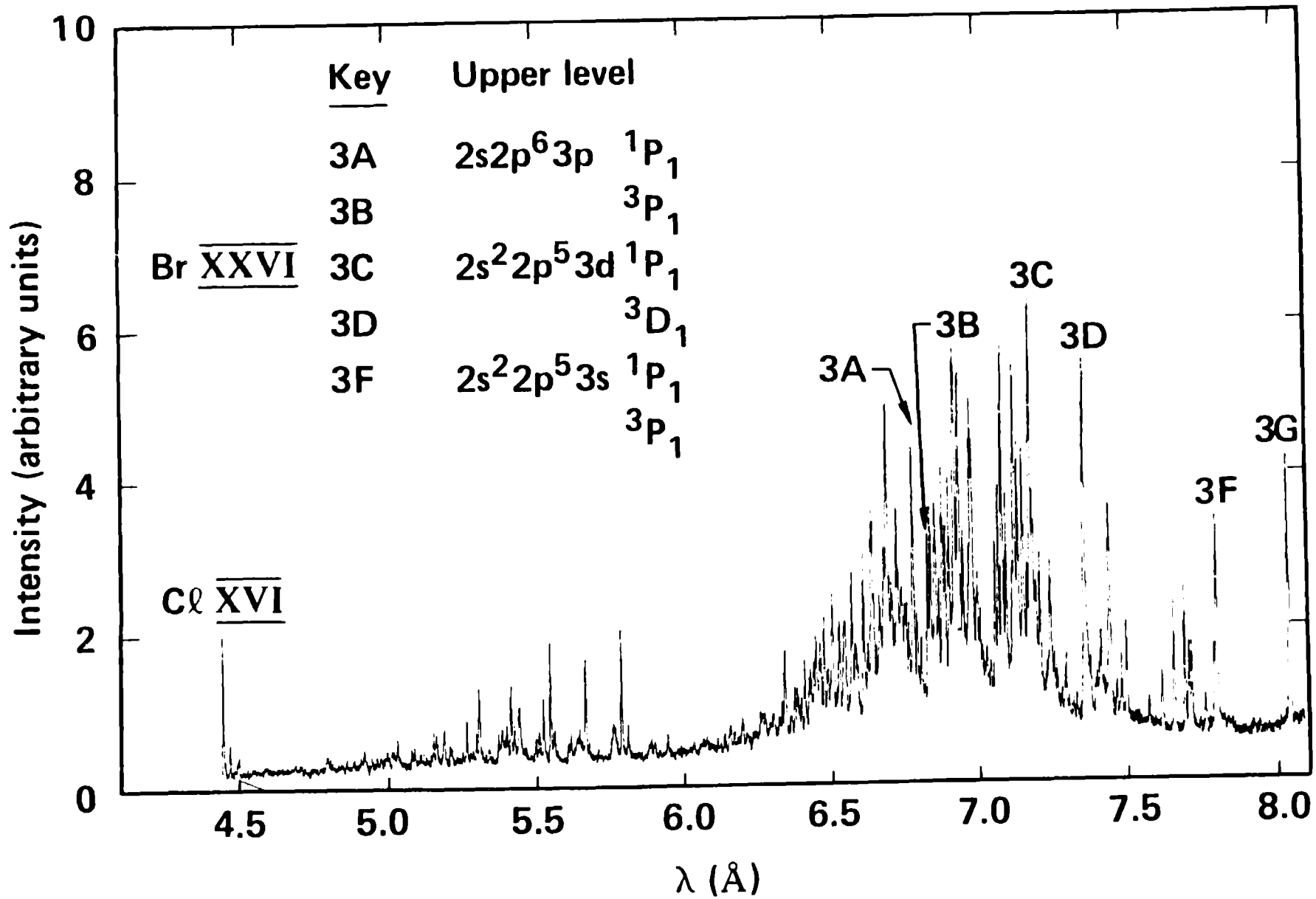
Key
Upper level
3A
2s2p⁶3p ¹P₁
3B
³P₁
Br XXVI
3C
2s²2p⁵3d ¹P₁
3D
³D₁
3F
2s²2p⁵3s ¹P₁
³P₁
3A
3B
3C
3D
3F
3G
Cℓ XVI
Intensity (arbitrary units)
λ (Å)
0
2
4
6
8
10
4.5
5.0
5.5
6.0
6.5
7.0
7.5
8.0

Fig. 5

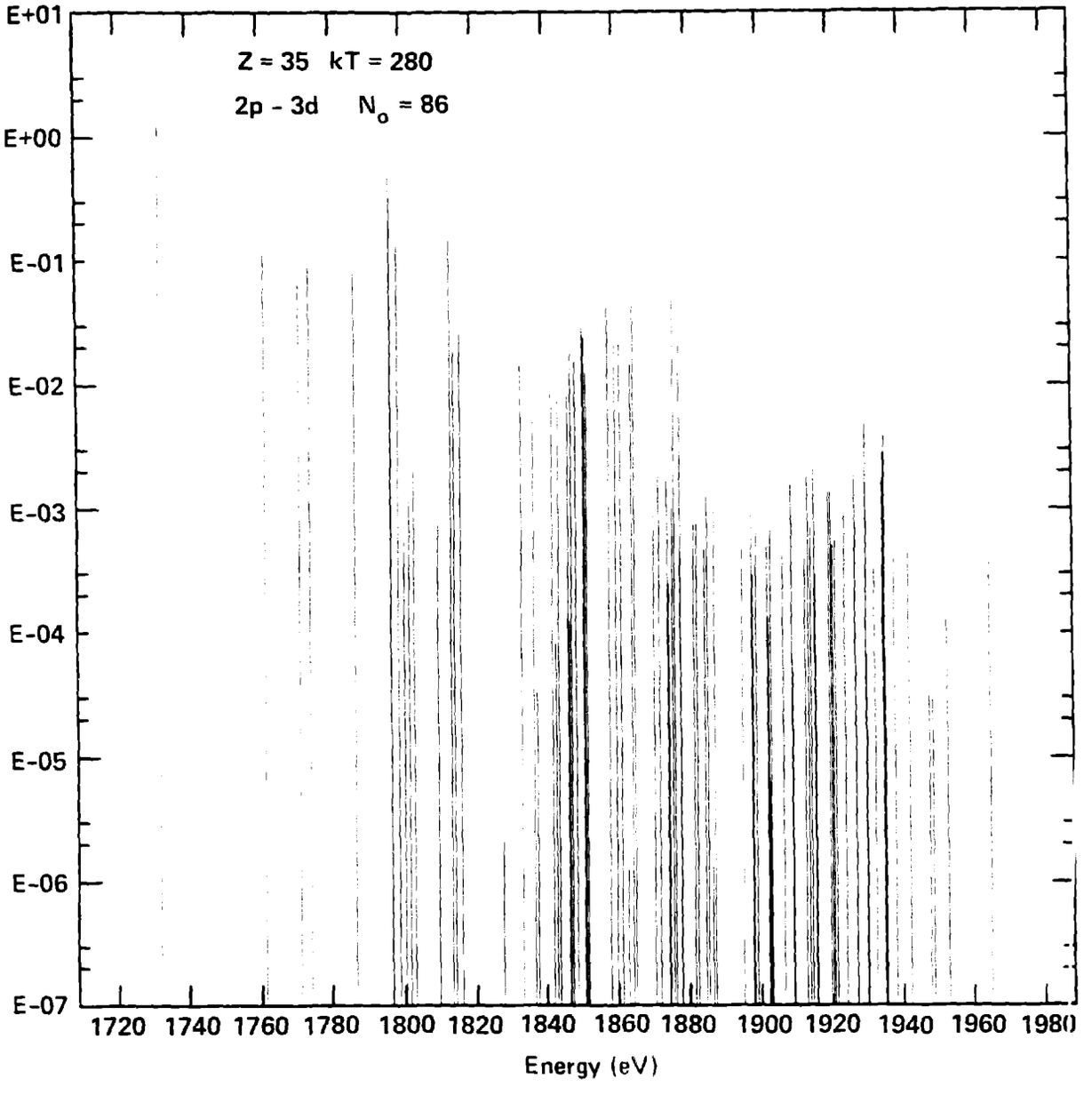
Z = 35 kT = 280
2p - 3d N$_o$ = 86
E+01
E+00
E-01
E-02
E-03
E-04
E-05
E-06
E-07
1720 1740 1760 1780 1800 1820 1840 1860 1880 1900 1920 1940 1960 1980
Energy (eV)

Fig. 6

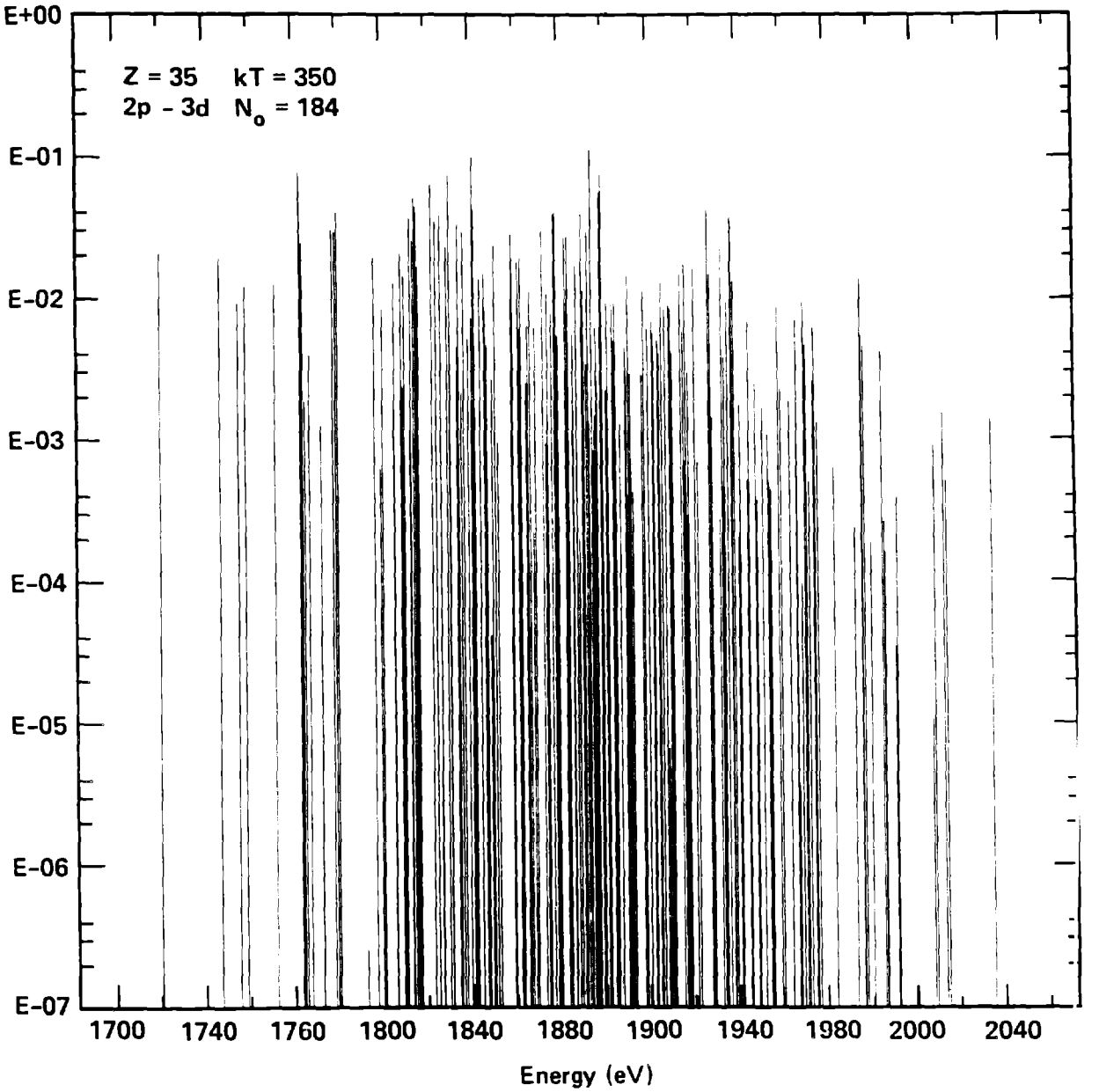
E+00
E-01
E-02
E-03
E-04
E-05
E-06
E-07
Z = 35 kT = 350
2p - 3d N$_o$ = 184
1700
1740
1760
1800
1840
1880
1900
1940
1980
2000
2040
Energy (eV)

Fig. 7

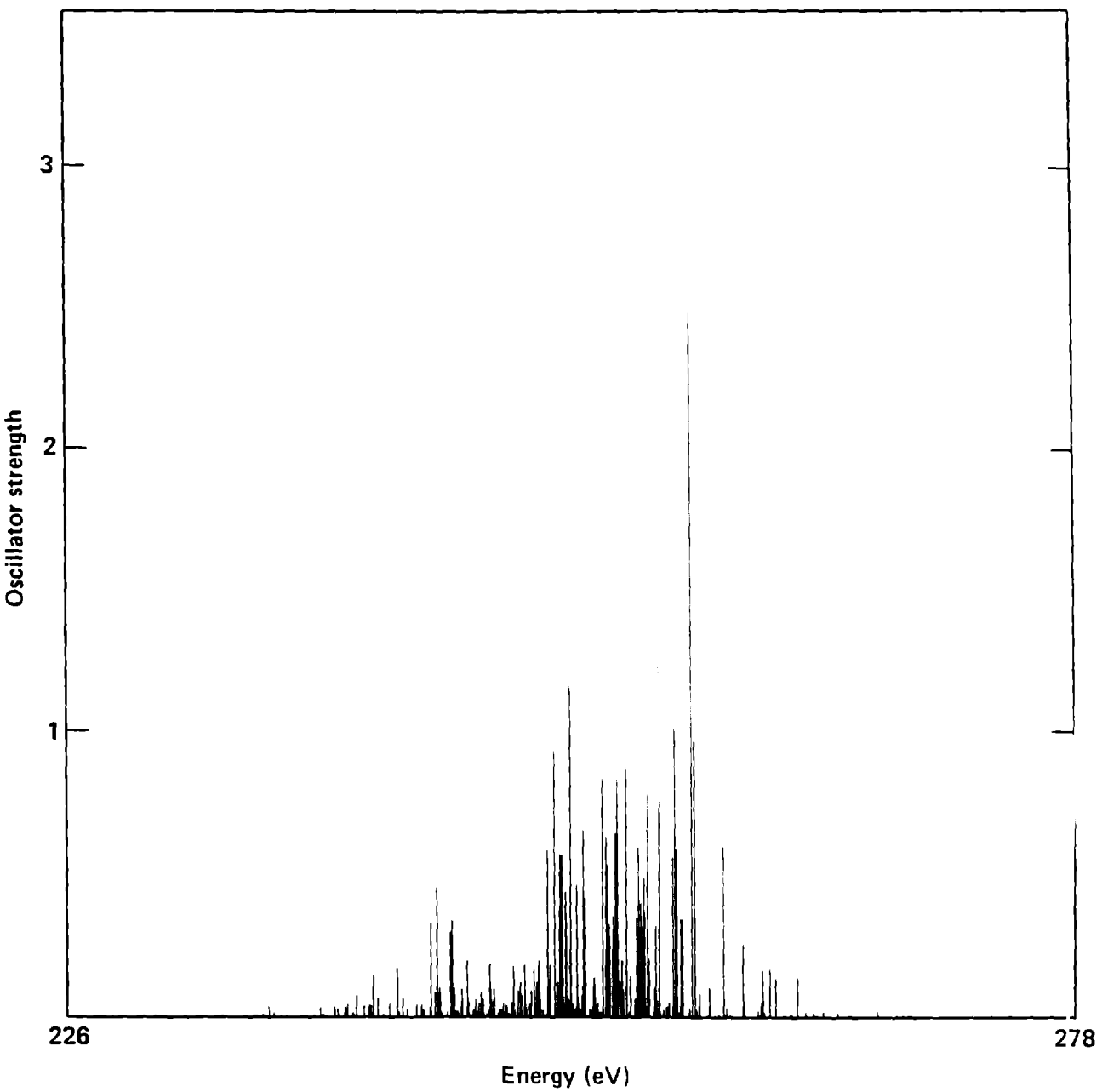

Fig. 8

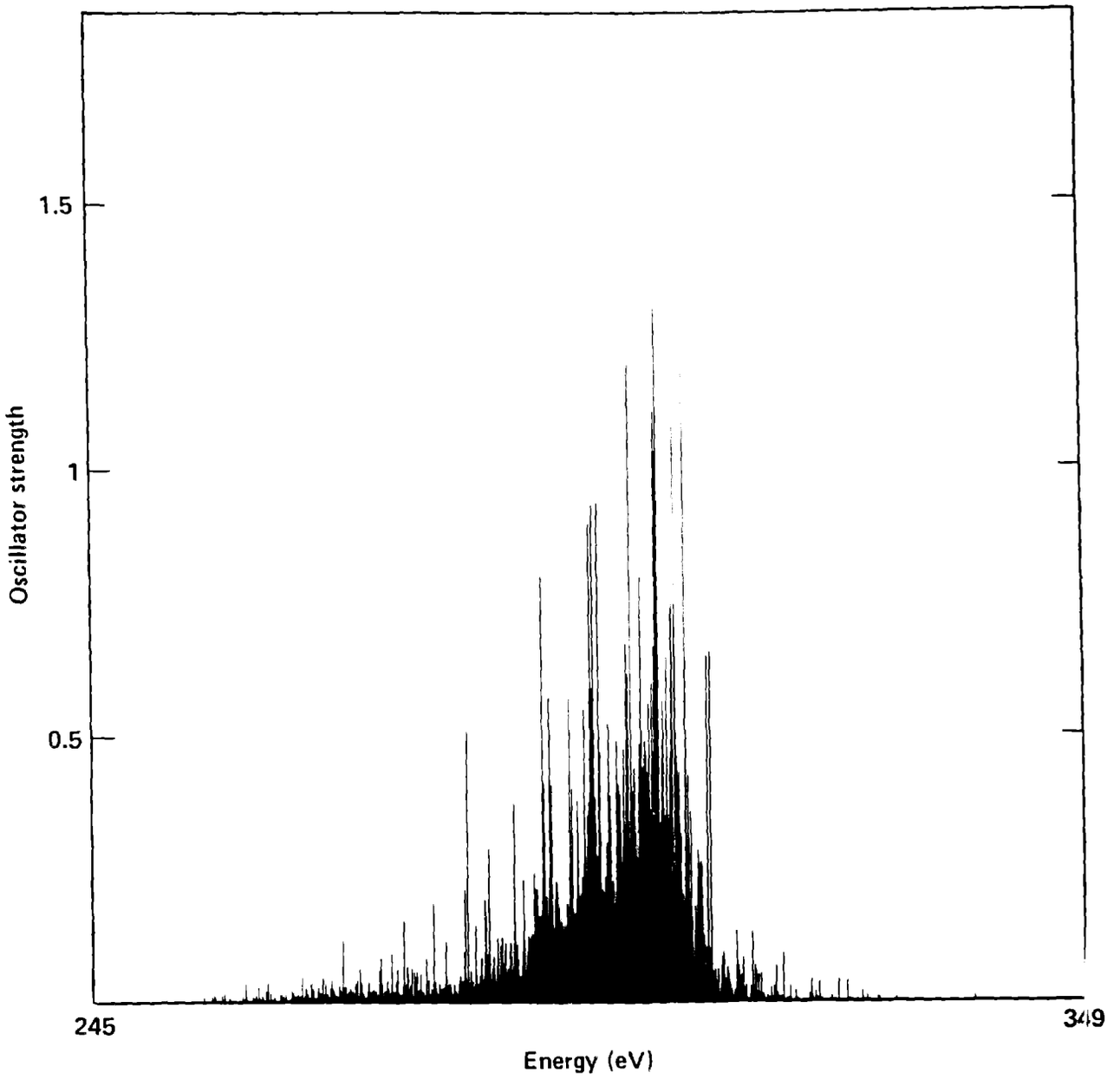

Fig. 9